

# Chirp Mitigation for Wideband GNSS Signals with Filter Bank Pulse Blanking

Alexander Rügamer, Shrikul Joshi, J. Rossouw van der Merwe, Fabio Garzia, Wolfgang Felber  
*Fraunhofer Institute for Integrated Circuits IIS, Nuremberg, Germany*  
Jan Wendel, Frank M. Schubert  
*Airbus Defence and Space GmbH, Germany*

## BIOGRAPHY

Alexander Rügamer received his Dipl.-Ing. (FH) degree in Electrical Engineering from the University of Applied Sciences Wuerzburg-Schweinfurt, Germany, in 2007. Since then he has been working at the Fraunhofer Institute for Integrated Circuits IIS in the Field of GNSS receiver development. He was promoted to Senior Engineer in February 2012. Since April 2013, he is head of a research group dealing with secure GNSS receivers and receivers for special applications. His main research interests focus on GNSS multi-band reception, integrated circuits and immunity to interference.

Shrikul Joshi received his MSc. degree in Electrical Engineering from the Technical University of Munich, Germany, in 2013. Upon graduation he joined the Fraunhofer Institute for Integrated Circuits IIS, where he is involved in signal processing for GNSS receiver including software and hardware development.

J. Rossouw van der Merwe received his B.Eng (Hons) and M.Eng. degrees in Electronic Engineering from the University of Pretoria, South Africa, in 2014 and 2016, respectively. He joined the Fraunhofer Institute for Integrated Circuits IIS in 2016, where his main research is in signal processing methods for interference mitigation and array processing applications.

Fabio Garzia received his MSc degree as Electronics Engineer from the University of Bologna, Italy, in 2005 and his Dr.Tech. (PhD) degree from the Tampere University of Technology, Finland, in 2009. From 2010 to April 2011, he received a research grant for the development of a high-level compiler for reconfigurable accelerators. In 2011 he joined the Fraunhofer Institute for Integrated Circuits IIS where he develops digital hardware and HW/SW interfaces for GNSS receivers targeting both ASIC and FPGA technologies. In May 2015 he was promoted to Senior Engineer.

Wolfgang Felber received his Dipl.-Ing. degree in Electrical Engineering in 2002 and his doctoral degree Dr.-Ing. in 2006 from Helmut-Schmidt-University of Federal Armed Forces Hamburg, Germany. Since 2014 he is head of the Power Efficient Systems department of Fraunhofer IIS in Nuremberg. The main topics in his department are energy harvesting and low power technologies, hardware development of satellite navigation receivers and sensor fusion in positioning applications.

Jan Wendel received the Dipl.-Ing. and Dr.-Ing. degrees in Electrical Engineering from the University of Karlsruhe in 1998 and 2003, respectively. From 2003 until 2006 he was an assistant professor at the University of Karlsruhe, where his research interests focused on integrated navigation systems and MAV flight control. Since 2006, he is private lecturer at the University of Karlsruhe. In 2006, Jan Wendel joined MBDA in Munich, where he was responsible for the design, implementation and test of target tracking filters for the Medium Extended Air Defense System (MEADS), and for the development of navigation algorithms for a tightly coupled GPS/INS system demonstrator. In 2009, he joined EADS Astrium GmbH in Munich, Germany, now Airbus DS GmbH, where he is involved in various activities related to satellite navigation including acquisition and tracking algorithms, compatibility analysis, interference detection and characterisation, GNSS/INS integration and integrity algorithms.

Frank Max Schubert graduated in 2007 in Electrical Engineering and Information Technology at the University of Karlsruhe, today's Karlsruhe Institute of Technology in Germany. From 2007 until 2011 he was member of the scientific staff at the Institute of Communications and Navigation of the German Aerospace Center (DLR). He worked partly in the Wave Propagation and Interaction Section at the European Space Agency (ESA) in Noordwijk, The Netherlands, within the Networking/Partnering Initiative from 2008 until 2010. From 2009 until 2012 F. M. Schubert was an external Ph.D. student in the Navigation and Communications Section at Aalborg University (AAU), Denmark. He obtained the Ph.D. degree from AAU in wireless communications in October 2012. Since November 2012 he is a system engineer for navigation signals at EADS Astrium GmbH in Munich, Germany, now Airbus DS GmbH.

## ABSTRACT

In this paper a filter bank pulse blanking (FBPB) approach is presented as a wide-band (WB) mitigation method for chirp-like interferences. This method uses a filter bank to separate the received global navigation satellite system (GNSS) signal in different sub-bands. As the WB chirp is broken into several segments, standard time domain pulse blanking (PB) can be used to mitigate this interference. Especially for wide-band GNSS signals – like higher-order binary offset carrier (BOC) modulated ones – the FBPB approach can be optimized so that at least one main-lobe is not effected by the blanking. Therefore, continuous signal tracking can be achieved with only moderate performance degradation. The method is analyzed, implemented and evaluated in both software and hardware GNSS receivers. Synthetically generated chirp interferences as well as recordings of commercial privacy protection devices (PPDs) are used to assess the performance of the FBPB in a software GNSS receiver. The hardware GNSS receiver implementation processes the interferences in real-time, demonstrating that this method is a practical solution to WB chirp-like signals.

## INTRODUCTION

Over the last few years, commercial jammers – such as personal or privacy protection devices (PPDs) – have become increasingly popular. These devices have also gained public attention due to several incidents of abuse and disruption of global navigation satellite system (GNSS) services. PPDs can be bought over the Internet, starting from 30 € for a plain car cigarette lighter powered jammer. For several hundred Euros a sophisticated all-band GNSS (including Global System for Mobile Communications (GSM) and Wi-Fi) jammers with external antenna connectors and configurable operation modes can be procured. GNSS band monitoring campaigns (e.g. [1]) have shown that these PPDs are used, despite being illegal in most countries<sup>1</sup>.

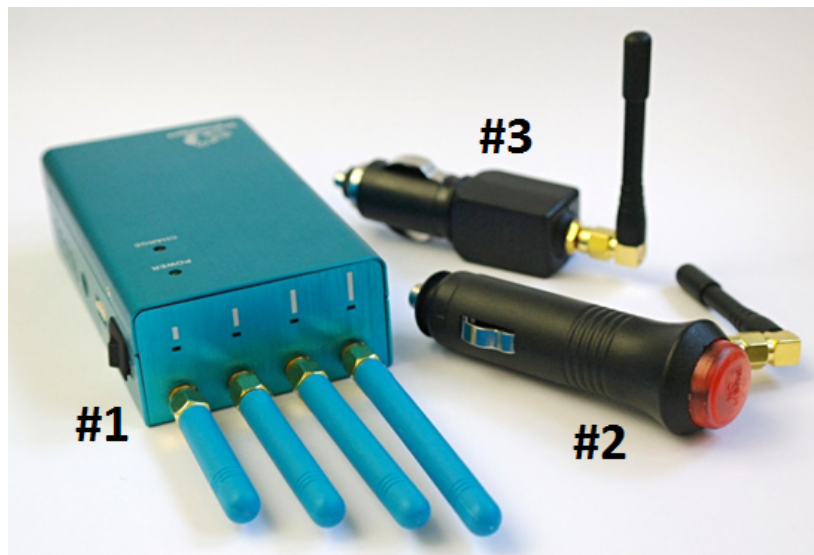


**Figure 1.** Photo of the PPDs used for evaluation

Commercially available jammers often transmit chirp-like signals (i.e. frequency modulated continuous waves (FMCWs)). Bandwidths from 1 to 45 MHz with sweep times from 8 to 20  $\mu$ s have been analyzed, with most of them situated around the L1 carrier frequency of 1575.42 MHz [2]. Wide-band (WB) chirp jammers with over 30 MHz bandwidth do not only affect the GPS C/A and Galileo open service (OS) signals, but also the GPS M-Code and Public Regulated Service (PRS) higher-order binary offset carrier (BOC) modulated ones.

In this paper, the concept of a narrow-band (NB) pulse blanking (PB) introduced by Borio in [3] is extended to WB receivers and signals. To receive the higher-order BOC modulated signals, like GPS M-Code L1/L2 BOCs(10,5), Galileo PRS E1A BOCc(15,2.5), Galileo PRS E6A BOCc(10,5) and Galileo E5 AltBOC(15,10), a reception bandwidth of up to 60 MHz is required. Therefore, the chirp signal can be considered as permanently being in-band to these higher order BOC signals, and basic NB chirp mitigation through PB will completely blank the GNSS signal. However, the spreading of the higher-order BOC modulated GNSS signals over the reception band results in a significant part of the GNSS signal (i.e. one of the two main-lobes) to be always unaffected by the chirp. This allows a temporary blanking of one of the side-bands together with a flexible full- and single side-band (SSB) processing.

<sup>1</sup>Transmitting in any frequency band in the electromagnetic (EM) spectrum without authorization is illegal; however, this does not stop the manufacturing of transmitters or jammers.

A filter bank pulse blanking (FBPB) is proposed, designed and tested in this paper, both in a software-defined radio (SDR) GNSS receiver as well as in a real-time hardware implementation on an field-programmable gate array (FPGA). An analog bandwidth of approximately 60 MHz is used in the implementations, such that Galileo E1 OS BOC(1,1) and E1 pseudo-PRS signals with a BOCc(15,2.5) modulation can be mitigated against slow and fast chirp interferences. It is shown that with higher order BOC signals, efficient mitigation can be performed. Consequently, tracking of the GNSS signals can still be achieved with moderate losses only, as long as the front-end is not saturated.

The paper is structured as follows: *Review of Chirp Jammer Mitigation* provides a review of current chirp mitigation methods, *Filter Bank Pulse Blanker* gives an introduction to PB design with the extension of using a filter bank. The simulation results using a SDR receiver are shown and discussed in *Simulations with Software GNSS Receiver*, and the results of a hardware implementation are outlined in *Hardware Receiver Test*. Finally, conclusions are drawn.

## REVIEW OF CHIRP JAMMER MITIGATION

The success of interference or jamming mitigation methods are largely dependent on the type of interference to suppress. Interferences that are sparse in the time or frequency domain are straight forward to mitigate: pulsed jammers can simply be blanked in the time domain, and stationary continuous wave (CW) jammers can be efficiently mitigated by applying a notch-filter. FMCW jammers (commonly perceived and referred to as chirps) are more difficult to mitigate, due to the constant transmission (i.e. no time domain blanking possible) and changing frequency (i.e. notch filter has to be adaptive if used). This leads to a high complexity of the interference mitigation implementation, with often only limited mitigation success. As a result, no practical and efficient signal processing approach against chirps has been reported yet.

The low quality design of commercial chirp jammers, with time-varying chirp characteristics (due to e.g. circuit imperfections and tolerances caused by the heating of the circuit and aging) further complicates the mitigation problem. An unpredictable interference source can be regarded as the worst case scenario, as no prior knowledge of the interference can be used to aid mitigation.

Sophisticated chirp mitigation methods, such as transforming the signal with interference to a domain where the interference has a sparse representation and then removing it, have been proposed [4]. Other methods use Wavelet or Karhunen-Loève-Transformation for interference mitigation [5]. However, these techniques are computationally complex and are not well suited for an efficient real-time hardware receiver implementation.

A more efficient method is an adaptive notch filter. However, if the sweep time of the chirp is sufficiently short (e.g.  $< 10 \mu\text{s}$ ) or if discontinuities in the interference signal appear (e.g. a step FMCW signal), an adaptive notch filter has limited mitigation capability [6]. This is due to the re-adaption phase of the filter after frequency discontinuities of the chirp signal within which the mitigation is non-existing or at least quite limited. The implementation of an adaptive notch filter in hardware can still be quite complex, especially when high sampling rates are required, as in the case for WB BOC modulated signals.

For NB GNSS receivers Borio [3] proposes to mitigate chirps though PB, which is a processing efficient and practical method, but only useful for a receiver with a small reception bandwidth relative to the chirp interference. If the frequency range swept by the jamming signal is significantly larger than the GNSS reception bandwidth of the receiver, the jamming signal periodically passes over the usable band. Therefore, the chirp signal is already filtered and suppressed by the receiver front-end. For the remaining in-band portion of the chirp, simple PB is proposed. Experiments have proven the effectiveness of this method. The limitation is that due to the NB operation, WB signals cannot be mitigated. This mitigation method is extended in this paper.

## FILTER BANK PULSE BLANKER

The new idea presented and discussed in this paper is the FBPB approach. The incoming signal band is split into multiple sub-bands using a filter bank consisting of finite impulse response (FIR) filters. For each sub-band a conventional PB is applied. The blanked sub-bands are combined, before standard GNSS processing is done. A block diagram of an exemplary three band FBPB is shown in Fig. 2.

If a chirp is present, only one of the sub-bands is affected – and consequently blanked – while the other sub-bands are unaffected. This approach of the FBPB exploits the frequency-selectivity of the chirp, as well as the frequency-diversity achieved by higher-order BOC signals. The following subsections discuss the parts required for FBPB.

### *Pulse Blanker*

It is well known that the degradation caused by pulsed signals are minimal, if the PB is applied and done correctly [7]. This explains how GNSS signals in the L5 band can coexist with distance measuring equipment (DME), even though DME systems transmits powerful – but short – pulses, with low pulse duty cycles (PDCs).

An efficient way to mitigate the disturbance effect on the GNSS signal tracking correlation process is to use a PB. A pulse blanker detects and nulls pulsed signals. This is done by comparing the amplitude of the signal to a threshold (pulse detector). If this

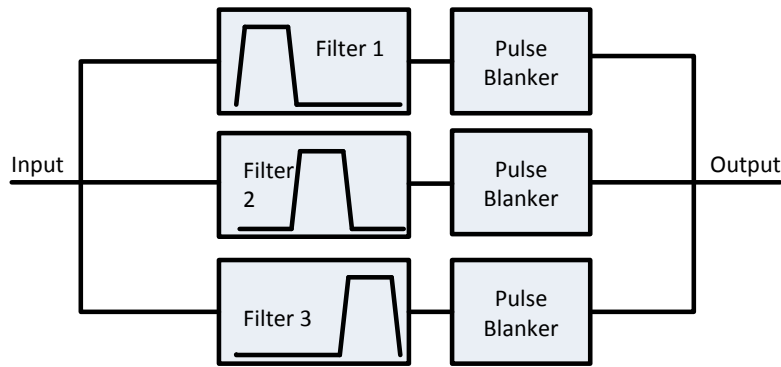


**Figure 2.** Block diagram of the FBPB architecture for an exemplary three sub-band configuration

threshold is exceeded, a pulse is detected and the corresponding samples of this pulse are replaced with zeros. If a pulsed signal was not blanked, the pulse power would increase the noise in the GNSS receiver's correlation process and consequently degrade its reception performance. Since most pulses are normally much shorter than the minimum integration time of 1 ms used in GNSS processing, the implementation loss of such a pulse blanking mitigation approach is negligible. A pulse blanker should also detect the length of the interference and only blank signals of short durations. For long duration signals, the blanker should switch to pass-through mode if the interference exceeds the predefined maximum blanking time. This avoids blanking of CW signals which else could lead to a complete switch off for an extended duration resulting in signal and significant performance losses. CW signals should be mitigated by different means, e.g. by applying a notch-filter.

The degradation of the effective  $C/N_0$  due to PB is only dependent on the PDC not on the actual pulse power, assuming the front-end shows no recovery effects when a strong pulse impinges the receiver, and the pulse blanker works ideally:

$$C/N_{0_{eff}} = C/N_0 \cdot (1 - PDC) \quad (1)$$

The comparison of the PDC to the  $C/N_0$  is shown in Fig. 3. Note that the 3 dB loss of  $C/N_0$  relates to a PDC of 50 %.

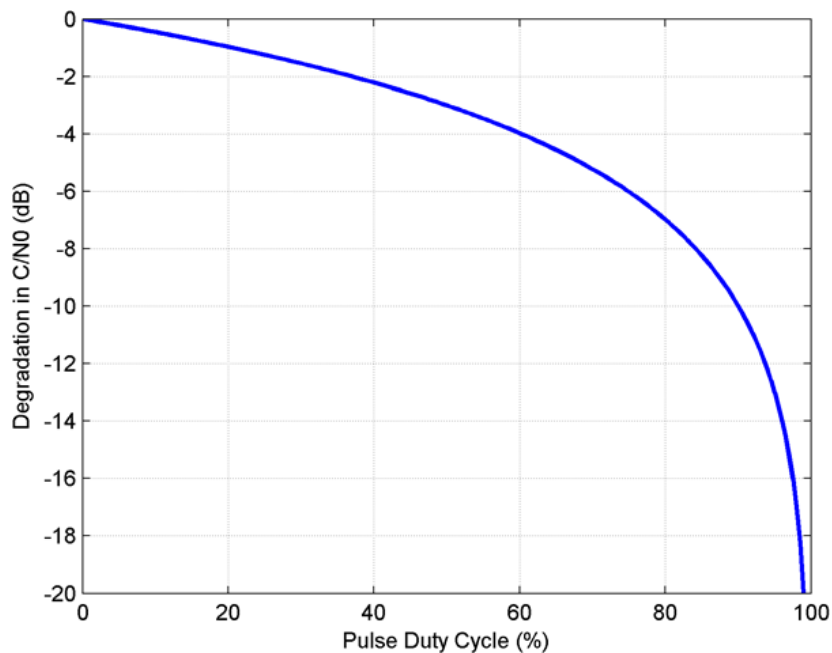


**Figure 3.**  $C/N_0$  degradation vs. blanked PDC

A feature of PB is that it is only a function of the temporal characteristics of the signal, hence a large interference to signal power ratio  $C_i/C_s$  will not reduce the mitigation ability. The disadvantage of PB is that for low  $C_i/C_s$  the detector cannot sufficiently detect the signal and as a result PB cannot be done. If the pulse detector is well designed and tuned, then only low  $C_i/C_s$  will be missed and the effects of the interferences has limited effect on the GNSS receiver. This shows that a good threshold setting for PB is important (i.e. tuning the threshold for a given scenario), as well as quality detector design. This may include implementing an energy detector over an amplitude detector [8], although this might cause latency issues in the system.

In the case of a NB PB, where the receiver front-end suppresses WB chirp signals [3], the chirp can be perceived as a pure pulsed signal. If it is assumed that the chirp has a spectrally flat response (i.e. it spends an equal amount of time at each frequency), the PDC of the pulse is the ratio between the bandwidth of the receiver (filter)  $B_F$  and the bandwidth of the chirp  $B_{chirp}$ <sup>2</sup>:

$$\text{PDC} = \frac{B_F}{B_{chirp}} \quad (2)$$

Consequently, for this case the effective loss of the C/N0 can be calculated as:

$$C/N_{0_{eff}} = C/N_0 \cdot \frac{B_{chirp} - B_F}{B_{chirp}} \quad (3)$$

### Filter Design

The sub-band filter properties directly influence the performance of the FBPB. The number of filters  $N_F$  and the number of coefficients  $N_C$  per filter relate to the complexity of the design, but also to their performance in out-of-band suppression and selectivity. The number of theoretical operations for the FBPB is  $O(N_C \cdot N_F)$ . The resources available for processing limit the number of operations, and consequently the number of filters and their coefficients. Further, for firmware or hardware implementations a word-length limitation exist if fixed point algorithmic is used<sup>3</sup>. Therefore, the quantization of the filter coefficients should also be considered.

The number of coefficients relate to how well the filter can be designed with the following parameters:

- pass-band ripple (in-band signal distortion)
- stop-band suppression (out-of-band signal suppression) – also referred to as the side-lobe level (SLL)
- transition between bands (full-band response, i.e. how close the filters can be placed)
- pass-band width (frequency filtering precision, also relates to the number of filters required)

The SLL is an important parameter in the FBPB, as it indicates the effectiveness of the sub-band isolation in relation to each other. In normal PB a signal is completely removed. However, if a signal with a high  $C_i/C_s$  is processed with a FBPB, then the correct filter will completely remove the signal, but all other filters will only suppress the interference by the attenuation of their SLL. Consequently, the interference cannot be completely mitigated, only suppressed. Therefore, it is critical to ensure a sufficiently high SLL in the filter design.

Figure 4 shows the SLL<sup>4</sup>(i.e. the stop-band suppression) vs. the number of coefficients at different quantization word lengths, for a fixed transition bandwidth of 4 MHz. For this filter design a sampling rate of 108 MHz is applied, since this is the target sampling frequency of the hardware receiver to be used for the implementation. Each point in the figure is a generated filter, where the designs are evaluated for their properties. The more coefficients used, the better the achievable performance, but at a certain point the limitation is the word-length. As an example, if the hardware can only use a word-length of 12 bit, then no more than 61 coefficients are required.

Figure 5 shows a similar approach, but this time the quantization length (meaning the word-length) is fixed at 16 bit, and the SLL is compared for different transition bandwidths and number of coefficients.

As illustrated a lower bound of the achievable SLL is present (the bound relates to the quantization of the filter coefficients). Designing them as close as possible to the bound will be optimal in terms of resource requirements for the filter design. This figure also shows the trade-off between how narrow a filter can be (therefore the transition bandwidth), with regard to the SLL of the filter, and the number of coefficients used.

### Filter Bank Design

The filter selection and design has a significant impact on the performance of a FBPB. The first step is to identify the signals which are to be processed by the GNSS receiver. For this paper the L1 / E1 band is considered with emphasis on the GPS C/A L1 (BPSK(1)), Galileo OS E1B/C (CBOC(6,1,1/11)) and Galileo pseudo-PRS E1A (BOCc(15,2,5)) signals. This provides a good indication for the placement of the filters. Ideally, a single FIR should be used per signal main-lobe, as a split of a main-lobe results in ripples and losses within the lobe. This limits practical designs to the use of three filters; for comparisons sake designs with more filters are considered in the software implementation. The blanking process of a design for three bands with different interferences is shown in Fig. 6. The Galileo OS and pseudo-PRS signals with the modulations mentioned above are also shown, as a reference.

<sup>2</sup>This is only true if  $B_F < B_{chirp}$ , and if the chirp transmits over the full receiver bandwidth  $B_F$ .

<sup>3</sup>Note that it is possible to use floating point operations in firmware or hardware. However, this is often inefficient and limits real-time signal processing capability.

<sup>4</sup>Note that this information will change according to the filter design method used, the quantization scaling, pass-band width, etc. The purpose of this figure is to illustrate the dependencies within the filter design.

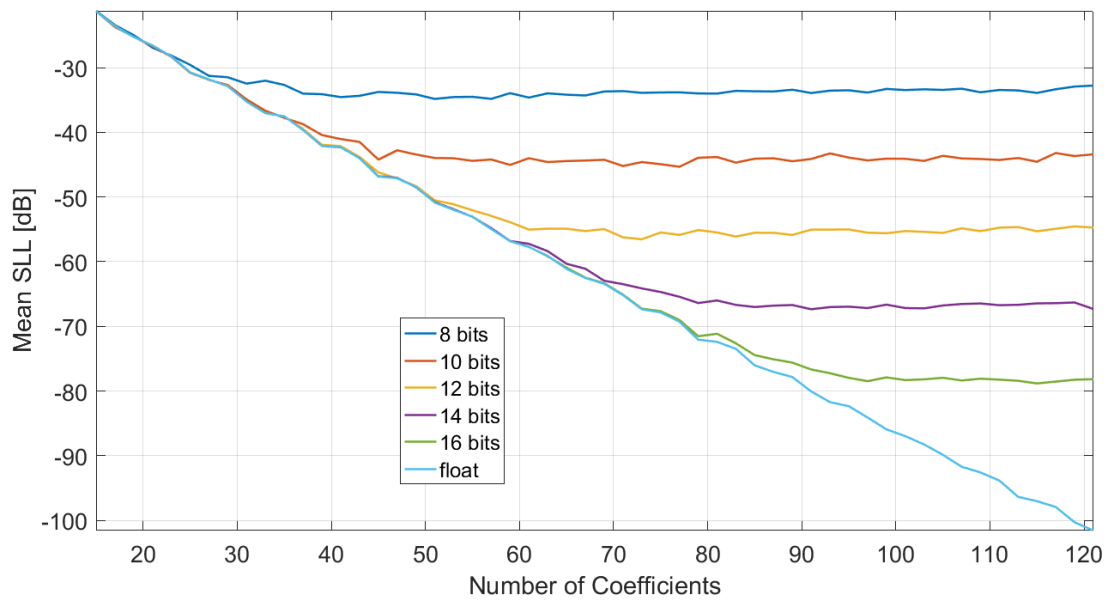


**Figure 4.** SLL comparison for different bit widths for a band transition width of 4 MHz

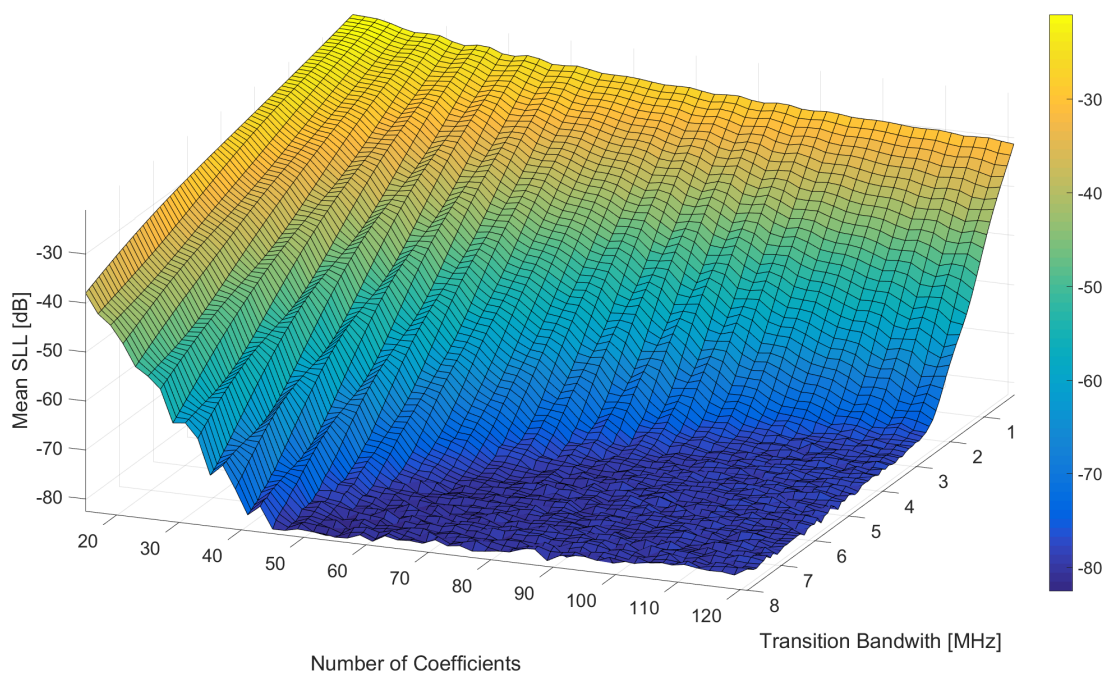


**Figure 5.** Filter design trade-off between SLL, band transition width and number of coefficients using 16 bit quantization

A second set of considerations are the front-end properties at the location of the FBPB implementation. The intermediate frequency (IF) in both the software and hardware implementations is assumed to be at zero frequency. The analog reception bandwidth is designed to be around 60 MHz for both software and hardware receiver investigations.

The number of sub-bands as well as their bandwidths are investigated in this paper. A summary of the design discussed in the section is displayed in Table 1. Note that the filter coefficients are quantized in the designs and implemented as such for both software and hardware implementations with a 16 bit word-length.

The designs of Table 1 for a sampling rate of 81 MHz<sup>5</sup> are shown in Fig. 7 Note that the SLLs for the designs are quite different, due to diverse design requirements (filter bandwidths, filter transitions bandwidths, pass-band rippling and number of coefficients) for each scenario.

For the Galileo E1 OS and pseudo-PRS signals of interest, three sub-bands with 10 MHz each is a practical choice (i.e. *Filter Design 1*, see Fig. 7(a)), as this will reduce the spectral noise in between the signals and limit unnecessary blanking. This is

<sup>5</sup>A sampling rate of 81 MHz relates to the software receiver.

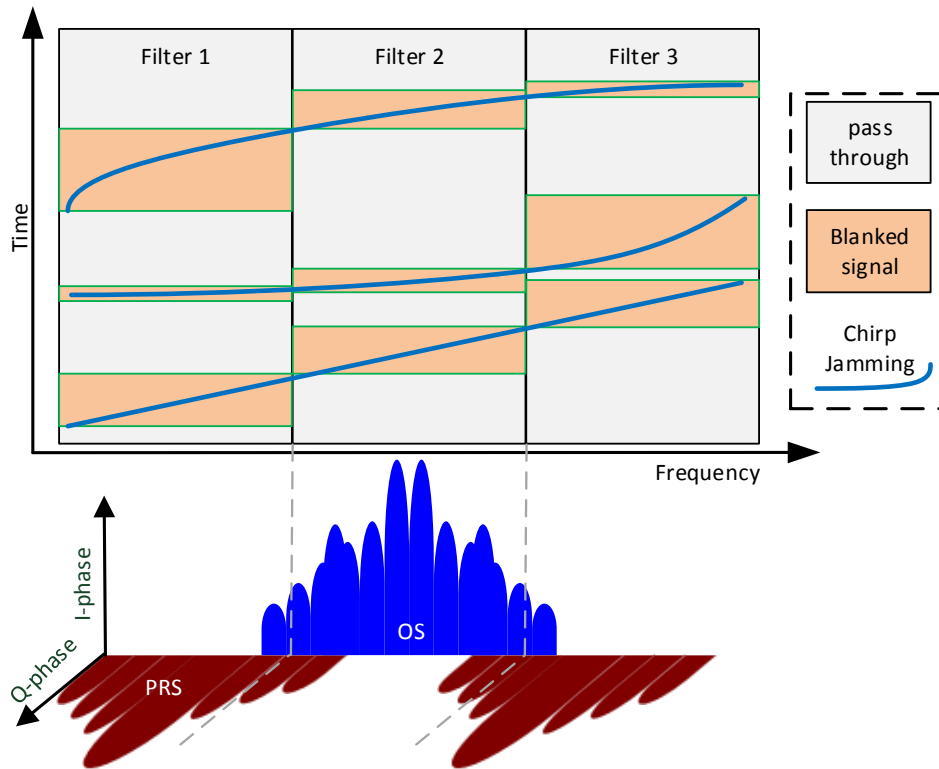


Figure 6. Visualization of the FBPB with a Galileo E1 OS/PRS example

Table 1. Filter designs evaluated

Design	Number of sub-bands	Filter bands (MHz)	Transition bandwidth (MHz)	Number of coefficients	Word-length (bit)
Filter Design 1	3	(-20, -10), (-5, 5), (10, 20)	4	42	16
Filter Design 2	3	(-20, -10), (-3, 3), (10, 20)	1	42	16
Filter Design 3	3	(-20, -8), (-8, 8), (8, 20)	4	42	16
Filter Design 4	3	(-30, -8), (-8, 8), (8, 30)	4	42	16
Filter Design 5	5	(-20, -10), (-6.5, -4), (-3, 3), (4, 6.5), (10, 20)	1	82	16
Filter Design 6	8	(-20, -15), (-15, -10), (-6.5, -4), (-3, 0), (0, 3), (4, 6.5), (10, 15), (15, 20)	1	162	16

also the design used for the majority of tests in the software implementation of the FBPB. Another method is to solely use the necessary spectrum (i.e. *Filter Design 2* and Fig. 7(b) of the Galileo OS / pseudo-PRS main-lobes (see Fig. 8)).

A flat spectrum design can be used to cover an assumed 40 MHz reception bandwidth without any bandwidth loss (i.e. *Filter Design 3* and Fig. 7(c)), hence a unitary filter design is required that allows minimal distortion to the un-interfered spectrum. This design can also be extended to the full analog bandwidth of 60 MHz (i.e. *Filter Design 4* and Fig. 7(d)). This has the benefit that no spectrum is lost, but interferences of non-critical frequencies forces PB over the whole sub-band, resulting in more signal loss during blanking. This filter design has additional constraints relating to the total band flatness, hence it results in increased SLLs for the same design methods. As what was shown in Eq. (3), the PDC increases as the bandwidth of the filter decreases, thereby, the effective C/N0 can also decrease if the filter banks are too large. The counter argument is that the broader the filter, the more of the GNSS signal can be used for tracking, resulting in a slightly better C/N0.

It is also possible to increase the number of filters to multiple bands (i.e. *Filter Design 5* and Fig. 7(e); or *Filter Design 6* and Fig. 7(f)). For these designs the number of coefficients should be increased to accommodate additional filter requirements

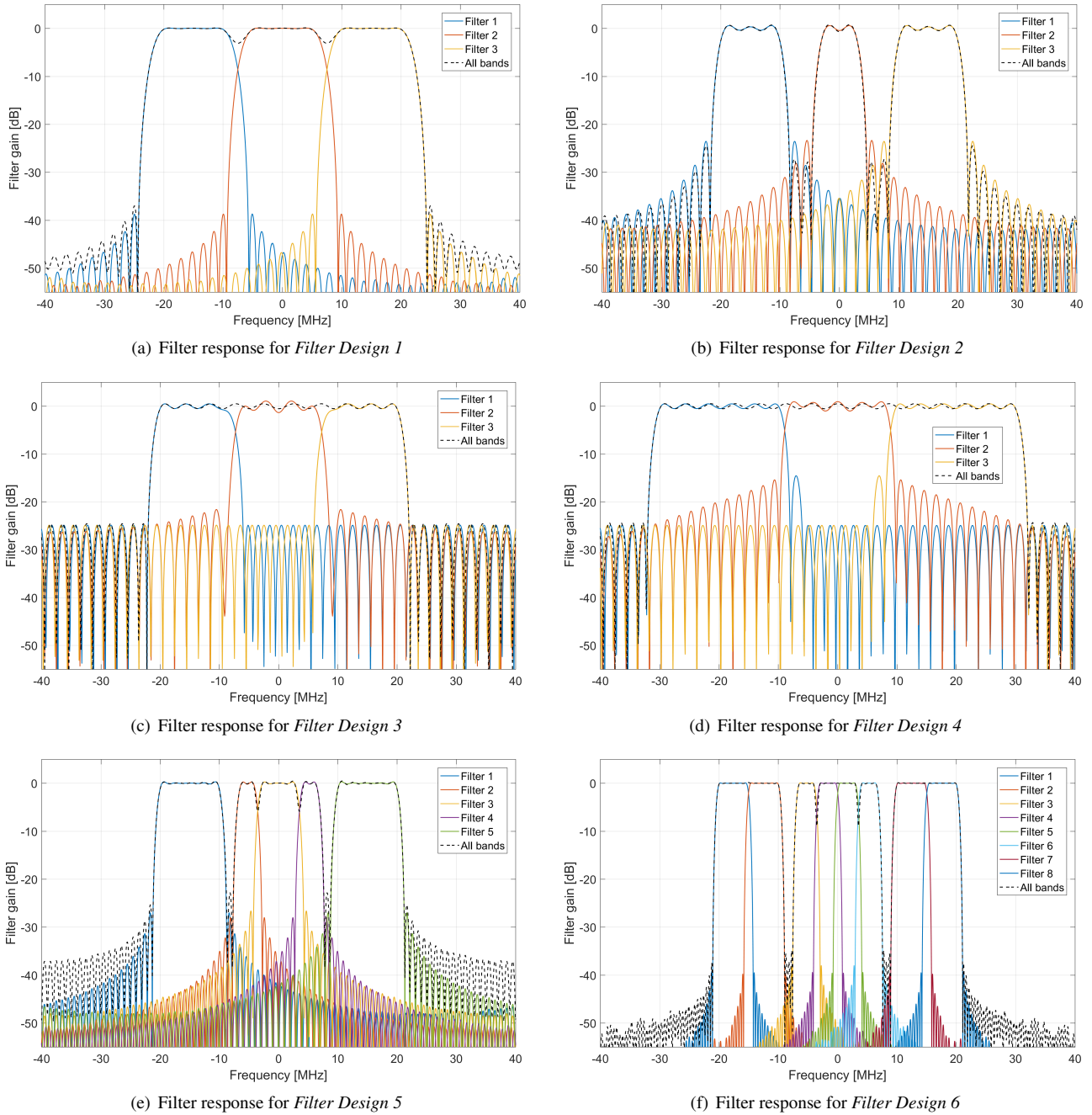


**Figure 7.** Different filter bank designs for a sampling rate of 81 MHz

of narrower transition widths and limited pass-band rippling. The number of sub-band filters as well as their selectivity and out-of-band suppression are related to the required FIR filter order (number of coefficients). This order is directly related to the resources required for realizing this FBPB approach. The trade-offs for a potential real-time FPGA hardware implementation should be considered. As stated earlier, if a main-lobe of a signal is split into multiple lobes, it may cause GNSS signal distortion resulting in additional  $C/N_0$  losses.

The benefits of a filter bank approach are that it can be efficiently implemented in hardware, it is independent of the interference type (e.g. chirp types or pulse interferences), and it can be optimized by adapting the FIR filters to the application required.

#### Theoretical Loss Derivation

The performance of the FBPB can be derived by expanding Eq. (3) for multiple filter bands. Assuming that for the derivation ideal brick-wall filters are used. Let the effective  $C/N_0$  only be attenuated by a factor  $L_{FB}$  from the interference (this relates to

the performance loss of the system), and a PB free C/N0:

$$C/N_{0_{eff}} = \frac{C/N_0}{L_{FB}} \quad (4)$$

The loss is the inverse of the signal power which is observed per filter band. Hence it is compounded by the power in each of the  $N_F$  filters. The fraction of the GNSS signal power  $F_s(n)$  of the  $n$ -th band is multiplied by the fraction of power where the interference is not present in the specific filter band<sup>6</sup>:

$$L_{FB} = \left[ \sum_{n=1}^{N_F} F_s(n) \cdot (1 - F_i(n)) \right]^{-1} \quad (5)$$

The fraction of the GNSS signal power  $F_s(n)$  in the  $n$ -th band is the ratio of the in-band power of the specified filter band (i.e. between the frequencies  $f_{start}^n$  and  $f_{stop}^n$ ) to the total power of the GNSS signal. This can be calculated by using the power spectral density (PSD) of the signal  $S_s(f)$ :

$$F_s(n) = \frac{\int_{f_{start}^n}^{f_{stop}^n} S_s(f) df}{\int_{-\infty}^{\infty} S_s(f) df} \quad (6)$$

The fraction of the power that a FMCW interference  $F_i(n)$  is in the filter band (resulting in the band as being blanked out), is related to the in-band power of the interference signal. Hence it can be calculated with the interference PSD  $S_i(f)$ :

$$F_i(n) = \frac{\int_{f_{start}^n}^{f_{stop}^n} S_i(f) df}{\int_{-\infty}^{\infty} S_i(f) df} \quad (7)$$

The PSDs for three different GNSS signals and three filters as used for *Filter Design 1*, are shown in Fig. 8.

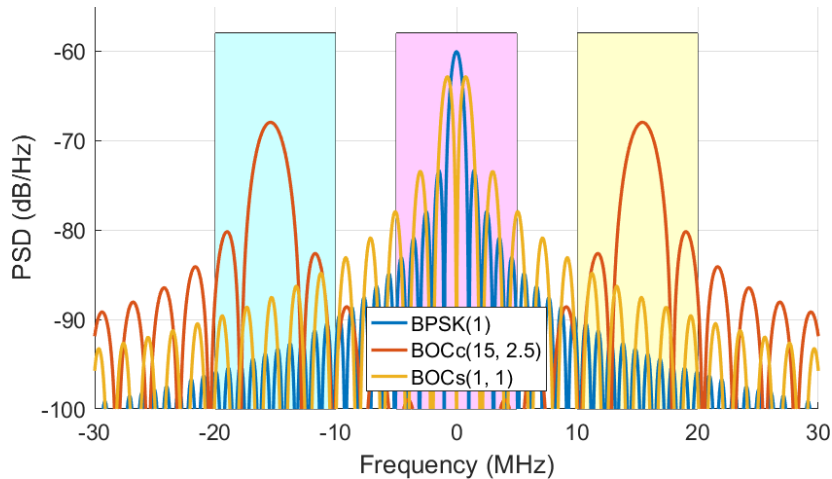


**Figure 8.** Spectrum of three GNSS signals with the location of three filters, used as an example for the theoretical performance derivation

The theoretical performance loss  $L_{FB}$  of the C/N0 is calculated for a flat spectrum chirp between -30 and 30 MHz and assumed ideal bandpass filters with bandwidths related to the six filter designs shown in Table 2. Note that this is the theoretical best achievable performance, as perfect filters and PB are assumed. Detection instabilities and filter non-idealities will increase the loss caused by this mitigation method.

<sup>6</sup>This is only true if a chirp signal with a constant signal envelope is assumed. The power in a frequency band of a FMCW signal relates proportionally to the time spent in the specified band.

**Table 2.** Theoretical FBPB losses for the different filter designs and a flat -30 ... 30 MHz chirp interference

Design	BPSK(1)	BOCc(15,2.5)	BOCs(1,1)
	Loss (dB)	Loss (dB)	Loss (dB)
<i>Filter Design 1</i>	0.9	1.0	1.9
<i>Filter Design 2</i>	0.6	1.0	0.9
<i>Filter Design 3</i>	1.4	1.2	1.4
<i>Filter Design 4</i>	1.4	2.0	1.4
<i>Filter Design 5</i>	0.5	1.0	0.7
<i>Filter Design 6</i>	0.3	0.6	0.5

## SIMULATIONS WITH SOFTWARE GNSS RECEIVER

The performance of the FBPB approach with different configurations is evaluated with a SDR GNSS receiver. The trade-offs between the number of sub-band filters vs. the number of coefficients for each filter are considered, as this assumes that an equal number of processing resources is available in hardware.

Galileo E1 OS and pseudo-PRS signals together with a WB chirp signal are recorded and processed. Different combinations of the FBPB are applied and the robustness of this approach is assessed in terms of C/N0 including loss of tracking with respect to the number and design of the sub-band filters.

### Test Setup

A Spirent GSS9000 radio frequency constellation simulator (RFCS) was used to generate a Galileo E1 signal with E1BC OS components, having a MBOC(6,1,1/11) modulation as well as a Galileo E1A pseudo-PRS signal with a BOCc(15,2.5) modulation. Thus, the real E1A PRS signal is substituted by pseudo-PRS or PRS-noise signals, while the E1A PRS modulation of BOCc(15,2.5) is preserved. The E1A pseudo-PRS pseudo random noise (PRN) chips are generated using the unclassified GPS P-Code. A static scenario with a nominal C/N0 of approximately 47 to 49 dBHz – depending on the elevation of each satellite – was used.

The output signals of the RFCS are received and stored to hard disk by the Flexiband USB3.0 front-end of Fraunhofer [9], using a configuration with 81 MHz sampling rate at 4 bit I/Q quantization.

For the signal evaluation, the PIPE GNSS SDR receiver of Airbus is used [10]. This receiver can track both the OS modulated Galileo signals, as well as the BOCc(15,2.5) modulated ones by obtaining the PRN-codes from a pregenerated pseudo-PRN-code file. To track the BOCc(15,2.5) signals, the Astrium-Correlator [11] is used, as it ensures that the main-peak is tracked and actively mitigates false locks on side-peaks. Moreover, the Astrium-Correlator can also be configured for solely tracking the BOCc(15,2.5) code envelope – being a BPSK(2.5) modulation – which is required when activating the FBPB.

In this scenario, the FBPB is implemented in software. The recorded Galileo E1 file is read, the interference mitigated with the FBPB and then saved as a new file. This allows a separate evaluation of the performance of the receiver before and after mitigation.

### Interference Free Test: Forced Pulse Blanking

The C/N0 of a single channel E1A pseudo-PRS is used as the metric of performance evaluation. At first, no interference was added. The *Filter Design 1* filters of the FBPB are switched at regular intervals, to show the effective C/N0 due to the pulse blanking of different sub-bands. The C/N0 for a single channel is shown in Fig. 9, with the spectrum of the signal at the different locations.

For the first 5 s of tracking, all filters were in pass-through mode (i.e. deactivated pulse blanking), thereby the unmitigated performance can be evaluated and stable tracking can be achieved. For 5 to 10 s the upper side-band (USB) is blanked, and a reduction of 2 dB in the C/N0 is observed, since one main lobe of the pseudo-PRS signal is also blanked. For 10 to 15 s the middle side-band is blanked, and the C/N0 stays constant as it does not affect the signal currently being tracked. For 15 to 20 s the lower side-band (LSB) is blanked, and a reduction of 2.5 dB in the C/N0 is observed. The discontinuities when moving between the different filter configurations are caused by the C/N0 estimation of the receiver due to the abrupt change of the signal. This test shows that the receiver and the FBPB react as predicted.

### Software Generated Interferences

An artificial chirp interference file was generated in Matlab and added to the recorded Galileo E1A pseudo-PRS file in software. A linear chirp from -30 to +30 MHz was used, with a linear chirp rate of -600 MHz/ms. The power of the chirp was changed for different scenarios.

The pulse-blanker is set to a minimum pulse length of about 50 ns, as this results in a pulse length of 4 to 5 samples, depending on the sampling rate used. A maximum pulse length of 1.2 ms is selected, as this relates to a maximum pulse of slightly longer

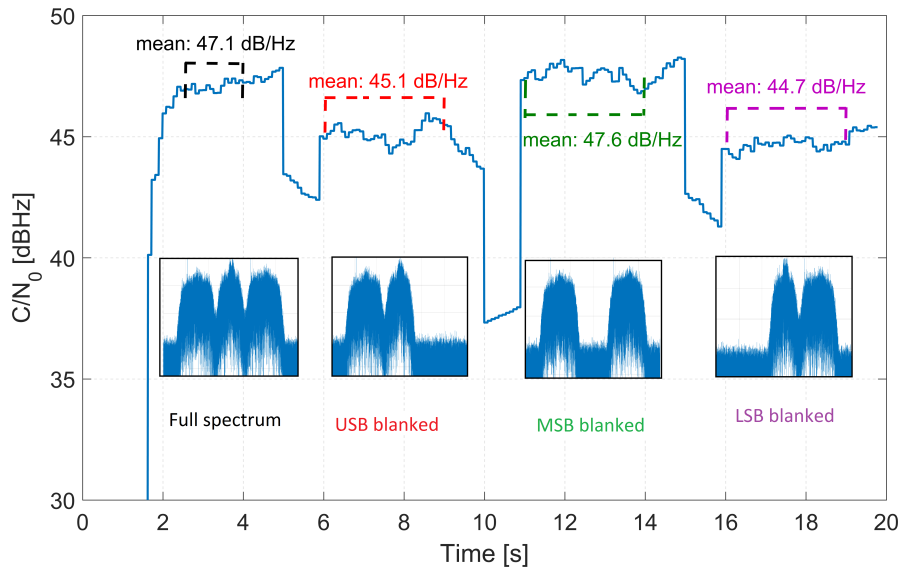


**Figure 9.** Forcing different sub-band filters into pulse blanking, to show the effective C/N0 in this mode of operation without interference

than one epoch for most GNSS signals. The standard deviation of the interference free signal is determined to be  $\sigma = 3.66$ , and the detector threshold is set to an amplitude value of 10. This relates to a single detection false alarm rate of 1.26%. A false alarm rate for a minimum pulse width of 4 samples is consequently  $25 \times 10^{-9}$ .

The waterfall display (spectrogram) before and after FBPB is shown in Fig. 10. *Filter Design 1* was used for this test. After the mitigation (Fig. 10(b)) it can be seen that the chirp is blanked out.

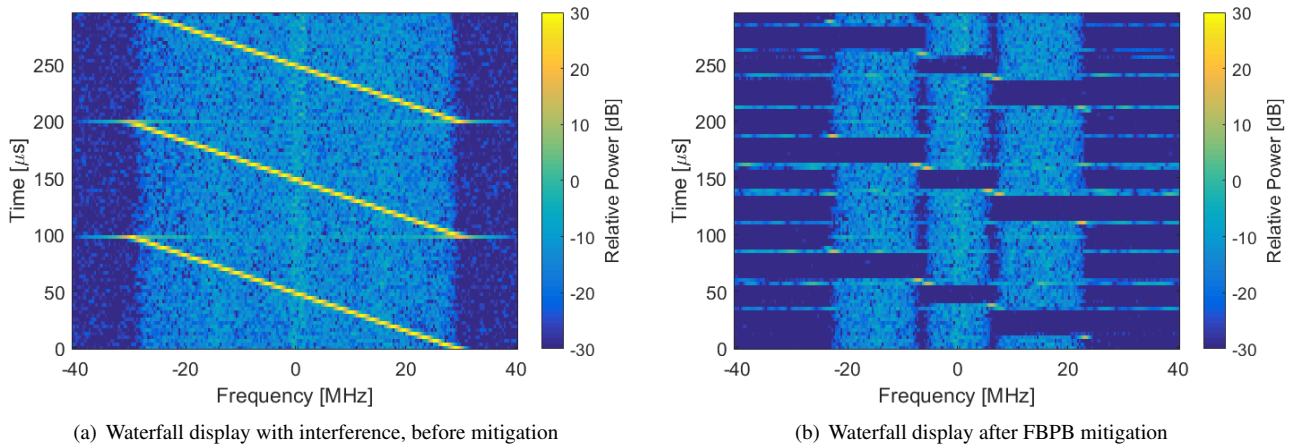


**Figure 10.** Waterfall display before and after FBPB mitigation

With each chirp repetition, the chirp is followed by the pulse blanker. This is shown by the three distinct blanked blocks in the spectrum, where the signals are nulled. Further, between the filter transitions, it can be seen that for a short period the chirp signal bleeds through. This is explained by the fact, that at the filter edges the power of the chirp is reduced, and as a consequence the detector does not reliably detect the interference. This is not considered as an issue, as the locations of these “bleed-throughs” are not at the same locations of GNSS signal main-lobes, and will therefore influence the GNSS minimally.

The filter masks can also be seen as the spectral response has a narrower pass-through range and the transitions between the filters are clearly lower. A final observation is that when the PB is turned on, the spectrum is temporarily distorted. This is explained by the discontinuity in the signal, which causes broad spectral distortion. The GNSS processing will not be affected by it, as this is primarily a visualization issue.

Figure 11 shows the waterfall outputs for the filters presented in Fig. 7. Here the masks of the different filters can be observed. Further the effects of the SLL “bleed-through” can clearly be seen as the chirp moves between the bands. Although these waterfall displays provide a good understanding on what is done with the signals, they do not show the performance of the GNSS receiver.

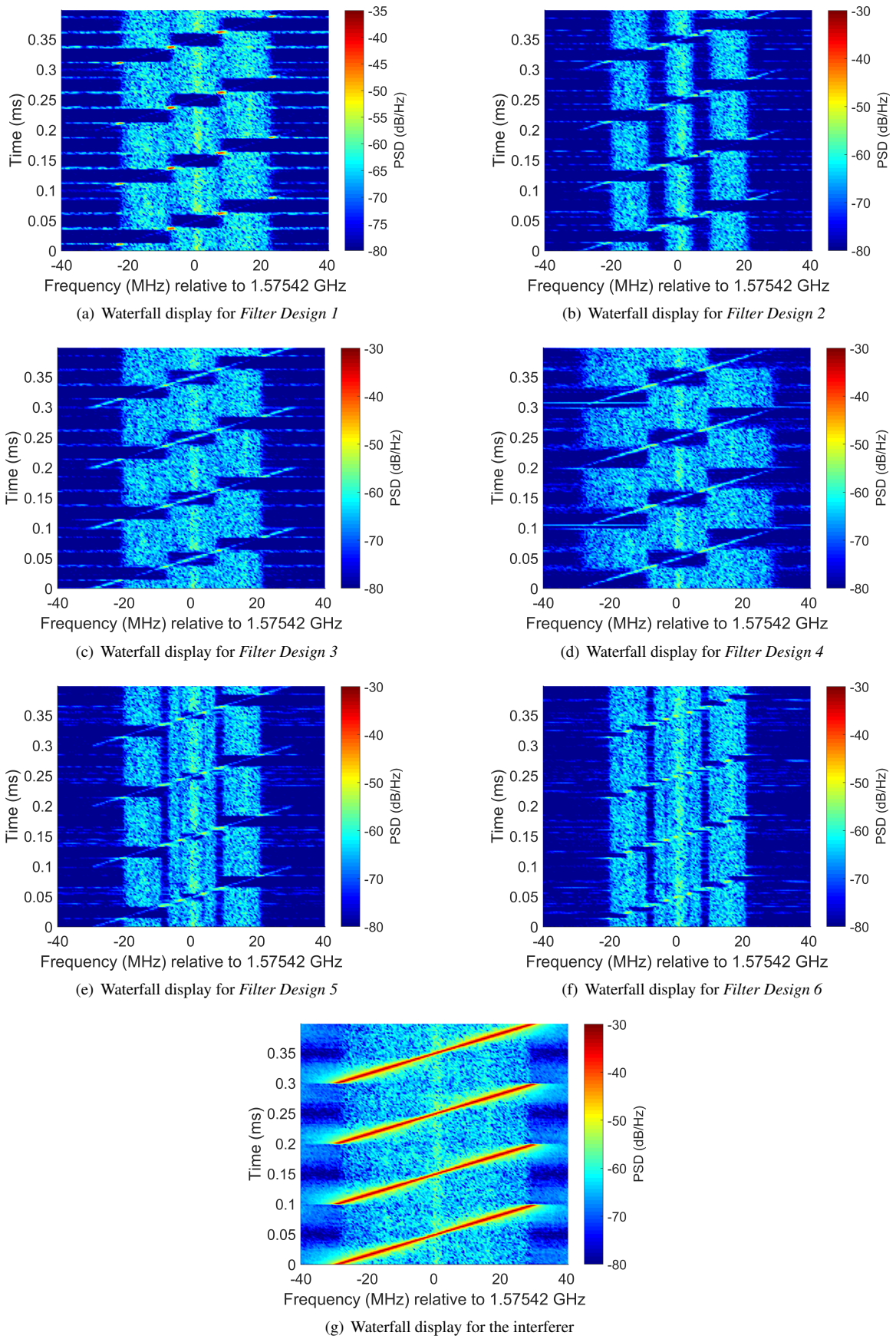


**Figure 11.** Waterfall displays for different filter designs after FBPB mitigation

The  $C/N_0$  estimation after tracking of the Galileo E1A pseudo-PRS, for the different FBPB filter designs is shown in Fig. 12. The chirp is switched on at 5 s, as this allows the GNSS signal to be in stable tracking conditions including a valid  $C/N_0$  estimation. Note once again that the “jumps” in  $C/N_0$  between 5 s and 6 s are unwanted artefacts of the  $C/N_0$  estimator used. The legend contains the average  $C/N_0$  estimated values between 7 s and 20 s when the FBPB mitigation is activated. This figure shows that all FBPB designs have a clear advantage with regard to the unmitigated case when the chirp is present, with a minimum increase of 10 dB in the  $C/N_0$  for this scenario<sup>7</sup>.

The different FBPB designs have an approximate 3 dB difference showing that the filter bank selection has a significant influence on the performance. An interesting observation is that the 8 band design (*Filter Design 6*) has poor performance if there is no interference present. This is caused by the distortion of the main-lobes of the GNSS signal by the filter overlap.

The best performing FBPB is using *Filter Design 1*, where the average  $C/N_0$  improvement in comparison to the unmitigated case is nearly 13 dB. The *Filter Design 3* is approximately 3 dB worse, due to the fact that the signal is blanked for a longer period and the filters have less out-of-band suppression.

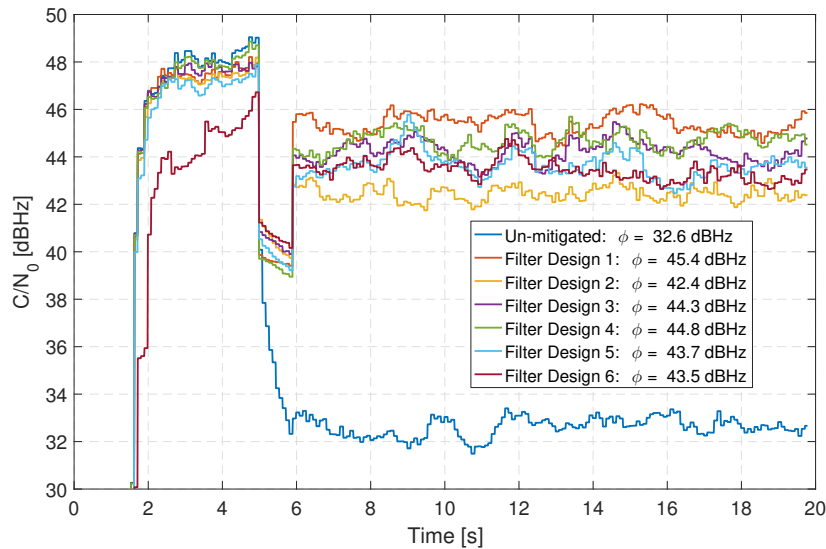


**Figure 12.**  $C/N_0$  comparison for different filter designs

For all subsequent tests, the FBPB with three filters is selected (i.e. *Filter Design 1*, Figs. 7(a) and 11(a)). The (-30, +30) MHz linear chirp is varied in its power and the  $C/N_0$  of the tracking output before and after mitigation is compared. The results are shown in Fig. 13: The unmitigated  $C/N_0$  decreases linearly with the increase of the estimated jammer or interference to noise ratio (INR), as expected by the theory.

For low INR values (1 to 6 dB), the pulse detector does not detect the interference and consequently no PB is done. In this case both the mitigated and unmitigated signals have similar performance. At medium INR values (6 to 10 dB), the pulse detector is in a transition region between no detections and good detections. This unreliability causes unpredictable signal blanking resulting in varying performance in this region. The mitigated  $C/N_0$  shows great improvement with high INR (10 to 22 dB), thereby showing the benefit of using the method. For very high INR (22 to 25 dB), the improvement of the FBPB starts to slope down. The interference starts to “bleed-through” the side-lobes of other filters, and consequently is not mitigated sufficiently. This stresses again that the performance of this interference mitigation method is directly linked to the achievable out-of-band suppression of the filters used.

#### Recorded Interferences

Three different commercial off-the-shelf (COTS) PPDs displayed in Fig. 1 where recorded in a laboratory setup. This allows the PPDs to be analyzed digitally and be used as an interference source for the software implementation. The PPDs are jammers which were all bought over the Internet, demonstrating how easy it is to purchase such a device. All three devices transmit chirp signals.

Again, the Flexiband USB data recorder was used to record the chirp interferences with deactivated “automatic gain control”. 60 dB of attenuation were inserted between the output of the chirp and the data recorder, as this ensures that the recording front-end is not saturated.

For the first 10 s the jammer was turned off, then switched on. The PPDs signals were added to the GNSS recordings, and then mitigated using FBPB with *Filter Design 1*. Fig. 15 shows the waterfall outputs before and after FBPB of the three PPDs. The

<sup>7</sup>The  $C/N_0$  improvement is highly related to the interference type, power and signal being tracked, hence these values are only valid for this specific scenario.

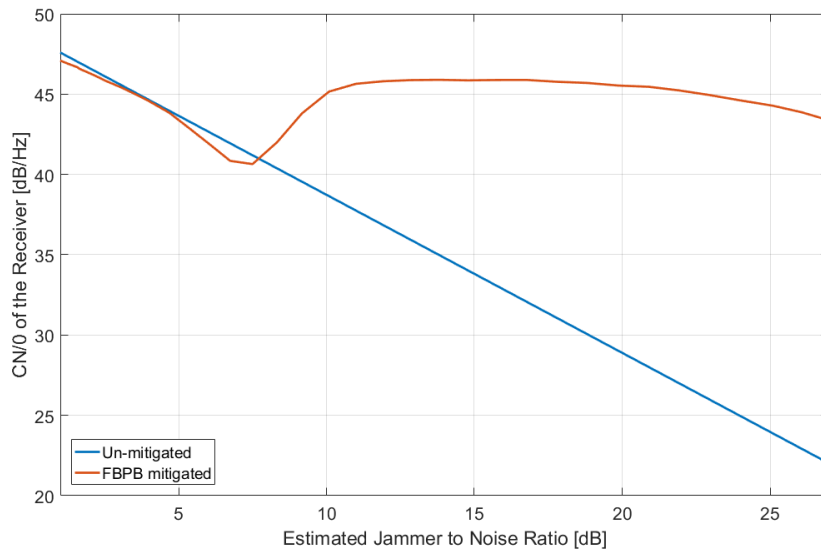


**Figure 13.** C/N0 comparison for a chirp jammer power sweep with and without FBPB mitigation, for a BOCc(15,2,5) GNSS signal

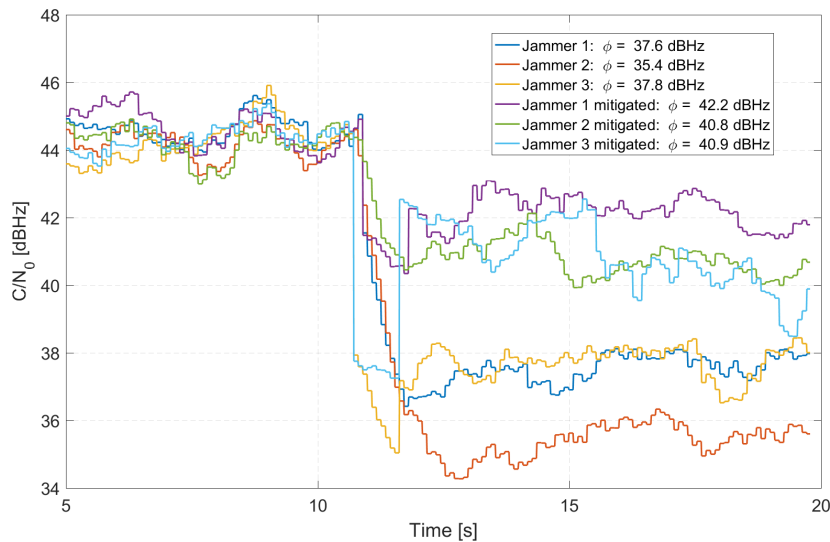


**Figure 14.** Jammer comparison with and without FBPB

tracking C/N0 output of the different PPDs are shown in Fig. 14.

The estimated jammer/interference to signal and noise ratio INR is 15.1 dB for Jammer 1, 14.8 dB for Jammer 2 and 12.1 dB for Jammer 3. These values, in conjunction with the output presented in Fig. 14, similar results are achieved as what was shown in Fig. 13. The interferences have different interference bands and consequently different PSDs, therefore some performance differences are expected.

## HARDWARE RECEIVER TEST

The pseudo-PRS BOCc(15,2,5) tracking has also been implemented on an FPGA-based receiver, using a sampling rate of 108 MHz and a 14 bit quantization in the front-end. The digital signal conditioning as well as the FBPB together with the Astrium-Correlator-based tracking channels were implemented into a Xilinx Zynq XC7Z045 system-on-chip (SoC) FPGA. A Linux operation system running on the internal ARM processor closes the tracking loops, using the PIPE software receiver. This hardware-assisted software receiver is comparable to the architecture outlined in [12].

The filter response *Filter Design 1* for the hardware implementation is shown in Fig. 16. The FPGA resource requirements for the design is shown in Table 3. Note that a complex valued filter design is used with 42 coefficients (i.e.  $4 \times 42 = 168$  digital signal processor (DSP) slices are required). All filters are configurable, therefore any of the 3-filter designs described above can be implemented on the same hardware and the design can be exchanged at run-time using software commands.

For the hardware experiment, the "Jammer 2" of Fig. 1 was used. This jammer has the highest sweep bandwidth of approx.

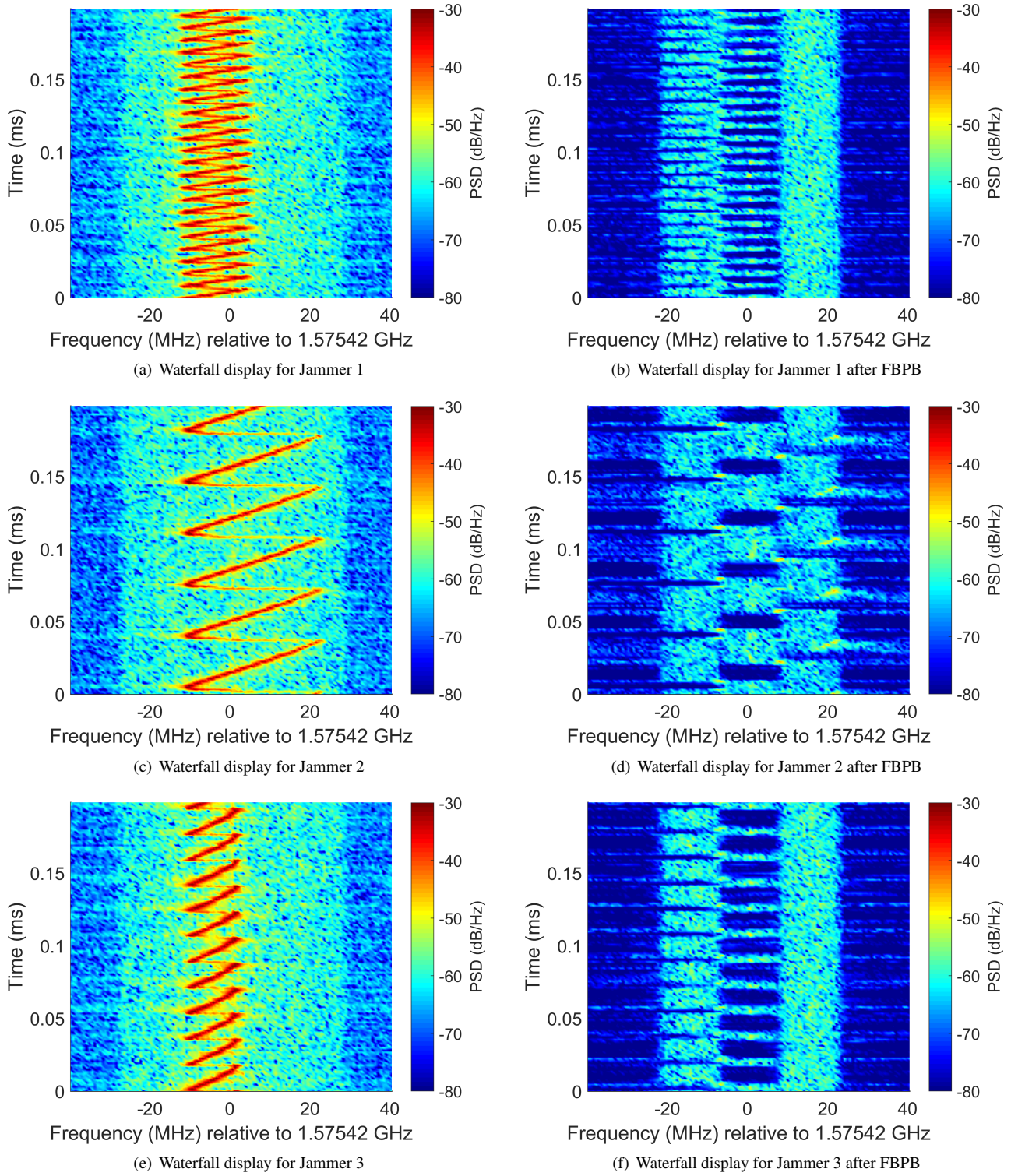


**Figure 15.** Waterfall displays for PPDs before and after FBPB mitigation

**Table 3.** Resource requirements on a Xilinx Zynq XC7Z045 SoC for a FBPB with three filters, 42 complex coefficients each

Resource	Per Filter		Full design	
	Amount	Percentage	Amount	Percentage
<i>LUT</i>	13 500	6%	41 000	18%
<i>FF</i>	21 500	5%	65 000	15%
<i>DSP blocks</i>	168	19%	504	56%

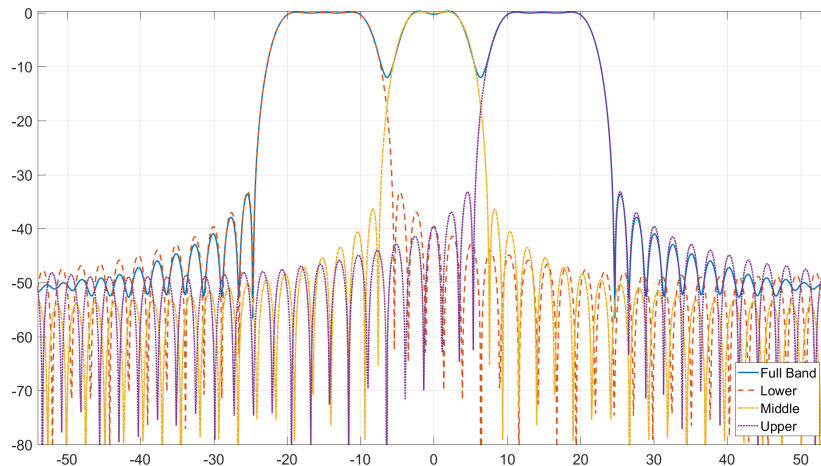


Figure 16. FBPB design after coefficient quantization

40 MHz and a measured output power of approx. +6 dBm directly at its antenna port. For the experiment, the antenna was removed. Instead, a 90 dB attenuator was connected, before the jammed signal was feed to the hardware receiver input via a two-way splitter (insertion loss less than 1 dB).

At first, the jammer was turned off and the receiver started to track four E1A pseudo-PRS signals with a BOCc(15,2.5) modulation. After turning on the jammer with its 90 dB attenuated signal but without any interference mitigation activated, the receiver instantly lost lock on all signals.

Then the FBPB was activated. In the beginning, with the jammer turned off again, the receiver tracked the four signals at a C/N0 of approx. 47 dBHz, as shown in Fig. 17. Then the jammer was turned on. The C/N0 dropped by approx. 2.5 dB. The interference power was increased in increments of 15 dB by changing the attenuators accordingly. Between the changes, the jammer was always turned off to allow the receiver to recover its initial interference free tracking state. At 75 dB attenuation, the effect was the same as for the 90 dB case. With 60 dB attenuation, the C/N0 drop was approx. 5.5 dB. At 45 dB attenuation, the C/N0 dropped down to around 30 dBHz and the receiver struggled to stay in tracking. This seems to be the limit in this specific receiver configuration with the given filters used. It should be noted that the receiver itself was not saturated but the maximum stop-band suppression of the FBPB design used, as shown in Fig. 16, was less than 50 dB, limiting also the suppression range of the chirp mitigation.

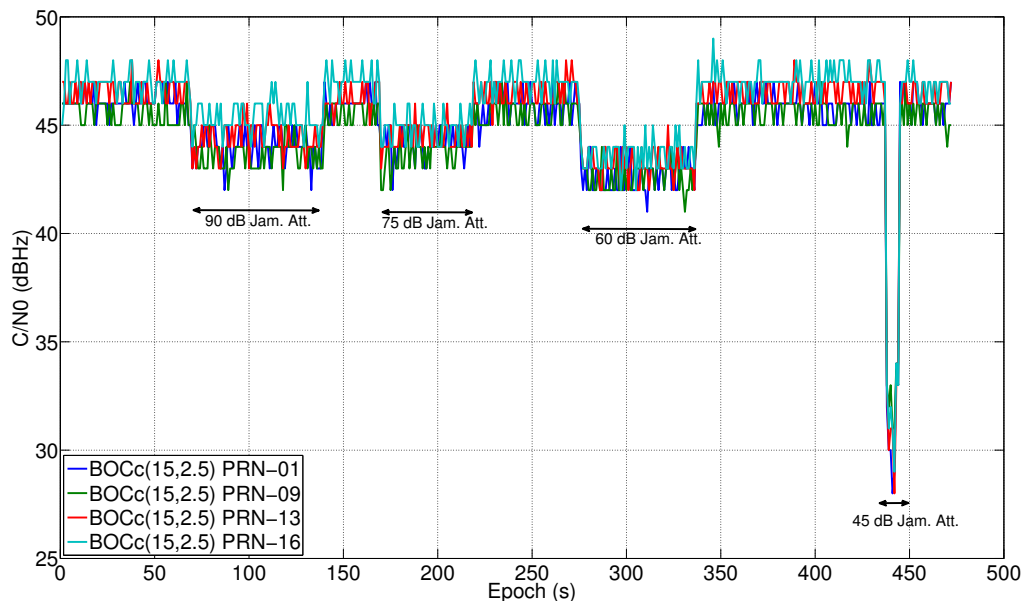


Figure 17. Hardware test of Jammer 2 with different attenuations

## CONCLUSION

Chirp interferences are a big threat to GNSS receivers as they are difficult to mitigate but easy to generate, making these signals the prime choice for jamming. Some mitigation methods exist against these attacks. In most cases, these methods have some constraints for a successful operation, like "well-behaved" or not too fast swept chirps.

The filter band pulse blanker (FBPB) method described in the paper has none of these preconditions. As long as the stop-band of its filters have sufficient suppression and the receiver's front-end is not saturated, any type of powerful interference signal is blanked. However, a wide-band GNSS signal (i.e. a higher order modulated BOC signal) is required to ensure a continuous tracking as well as tracking methods that are able to continuously process the signal when one or the other main-lobe being filtered out.

This FBPB method has been implemented and tested in both software and hardware receiver implementations. It was shown to be an effective mitigation method for wide-band GNSS signal receivers. The method has low implementation complexity, and is proven to be realizable in real-time. COTS PPDs have been recorded and used as a reference to evaluate the performance of FBPB.

A successful chirp interference mitigation of 45 dB interference power range of a real-world PPD has been demonstrated in a real-time FPGA GNSS receiver processing BOCc(15,2.5) modulated GNSS signals. The actual mitigation capability can be further improved by increasing the stop-band attenuation of the digital filters.

## REFERENCES

- [1] A. Rügamer, D. Meister, J. R. van der Merwe, C. Otto, M. Stahl, and W. Felber, "Versatile and Configurable GNSS Interference Detection and Characterization Station," in *Proceedings of the ION 2017 Pacific PNT Meeting*, May 2017.
- [2] T. Kraus, S. Sailer, and B. Eissfeller, "A Dual-Frequency Interference Suppression Unit for E1/E5a Designed with National Instruments Software Defined Radios," in *28th International Technical Meeting of the Satellite Division of The Institute of Navigation, Tampa, Florida, 2015*.
- [3] D. Borio, "Swept GNSS jamming mitigation through pulse blanking," in *2016 European Navigation Conference (ENC)*, pp. 1–8, May 2016.
- [4] A. Rügamer, I. Lukčín, G. Rohmer, and J. Thielecke, "GNSS Interference Detection using a Compressed Sensing Analog to Information Converter Approach," in *Proceedings of the 2013 International Technical Meeting of The Institute of Navigation - ION ITM 2013, January 28 - 30, 2013, San Diego, CA, 2013*.
- [5] L. Musumeci and F. Dovis, "A comparison of transformed-domain techniques for pulsed interference removal on GNSS signals," in *2012 International Conference on Localization and GNSS*, pp. 1–6, June 2012.
- [6] J. Wendel, F. M. Schubert, A. Rügamer, and S. Taschke, "Limits of Narrowband Interference Mitigation Using Adaptive Notch Filters," in *Proceedings of the 29th International Technical Meeting of The Satellite Division of the Institute of Navigation (ION GNSS+ 2016)*, September 2016.
- [7] C. Hegarty, A. Van Dierendonck, D. Bobyne, M. Tran, and J. Grabowski, "Suppression of Pulsed Interference through Blanking," in *Proceedings of the IAIN World Congress and the 56th Annual Meeting of The Institute of Navigation, San Diego, CA*, pp. 399–408, June 2000.
- [8] S. M. Kay, *Fundamentals of Statistical Signal Processing: Detection Theory*, vol. 2 of *Prentice-Hall Signal processing series*. Prentice Hall, 1998.
- [9] A. Rügamer, F. Förster, M. Stahl, and G. Rohmer, "A Flexible and Portable Multiband GNSS Front-end System," in *Proceedings of the 25th International Technical Meeting of the Satellite Division of the Institute of Navigation, ION GNSS 2012, September 17-21, 2012, Nashville, Tennessee, USA*, September 2012.
- [10] F. M. Schubert, J. Wendel, F. Soualle, M. Mink, S. Carcanague, R. Ioannides, P. Crosta, and M. Crisci, "Integrity of Navigation for Land Users: Study Concept and Simulator Architecture," in *Proceedings of 7th ESA Workshop on Satellite Navigation Technologies, Navitec 2014, Noordwijk, The Netherlands, 2014*.
- [11] F. Schubert, J. Wendel, S. M., M. Kaindl, and R. Kohl, "The Astrium Correlator: Unambiguous Tracking of High-Rate BOC Signals," in *Proceedings of IEEE/ION PLANS 2014, Monterey, CA, May 2014*, pp. 589–601, 2014.
- [12] A. Rügamer, P. Neumaier, P. Sommer, F. Garzia, G. Rohmer, A. Konovaltsev, M. Sgammini, S. Caizzone, M. Meurer, J. Wendel, F. F. Schubert, and S. Baumann, "BaSE-II: A Robust and Experimental Galileo PRS Receiver Development Platform," in *Proceedings of the 27th International Technical Meeting of The Satellite Division of the Institute of Navigation, ION GNSS+ 2014, September 8-12, 2014, pp. 2579-2591, Nashville, Tennessee, USA, September 2014*.